

Microscopic calculation of inelastic proton scattering off ^{18}O , ^{10}Be , ^{12}Be , and ^{16}C for study of neutron excitation in neutron-rich nuclei

Yoshiko Kanada-En'yo

Department of Physics, Kyoto University, Kyoto 606-8502, Japan

Kazuyuki Ogata

Research Center for Nuclear Physics (RCNP), Osaka University, Ibaraki 567-0047, Japan

Department of Physics, Osaka City University, Osaka 558-8585, Japan and

Nambu Yoichiro Institute of Theoretical and Experimental Physics (NITEP), Osaka City University, Osaka 558-8585, Japan

The microscopic coupled-channel calculation of inelastic proton scattering is performed for the study of neutron excitations in 2_1^+ states of ^{18}O , ^{10}Be , ^{12}Be , and ^{16}C . Proton-nucleus potentials in the coupled-channel calculation are microscopically derived by folding the Melbourne g -matrix NN interaction with matter and transition densities of target nuclei obtained by the structure model calculation of antisymmetrized molecular dynamics. The calculated result reasonably reproduces the elastic and inelastic proton scattering cross sections, and supports the dominant contribution of neutron in the 2_1^+ excitation of ^{12}Be and ^{16}C as well as ^{18}O . Sensitivity of the inelastic scattering cross sections to the neutron transition density is discussed. The exotic feature of the neutron transition density with the amplitude in the outer region in ^{12}Be and ^{16}C is focused.

I. INTRODUCTION

Shape difference in proton and neutron matter distributions in nuclei is one of the interesting phenomena in unstable nuclei. To discuss the difference between the neutron and proton deformation (or collectivity), the neutron and proton transition matrix elements in the ground-band $2_1^+ \rightarrow 0_1^+$ transition have been investigated for a long time. In a naive expectation for ordinary nuclei with the same proton and neutron deformation, the ratio of the neutron transition matrix element (M_n) to the proton one (M_p) should be N/Z . However, the relation $M_n/M_p \approx Z/N$ is not satisfied even in stable nuclei with the proton or neutron shell closure as reported in Ref. [1]. For instance, in ^{18}O and ^{48}Ca , the ratio becomes significantly larger than N/Z , which indicates the neutron dominance in the 2_1^+ excitation because of the proton shell closure. The phenomena of the shape difference and/or the neutron dominance have been suggested also in unstable nuclei such as ^{10}Be , ^{12}Be , and ^{16}C [2–15].

Experimental information of the proton part M_p can be directly obtained from the $E2$ strength. By contrast, determination of the neutron part (M_n) is not easy even for stable nuclei. Instead of direct measurements, experiments of inelastic hadron scattering have been performed using such probes as α , proton, neutron, and π^-/π^+ . By combining the hadron scattering data with the electromagnetic data, M_n and M_p have been discussed based on reaction analysis (see Refs. [1, 16] and references therein). For ^{18}O , the neutron matrix element of the $2_1^+ \rightarrow 0_1^+$ transition has been intensively investigated, and the anomalously large value of $M_n/M_p \approx 2$ has been reduced from the inelastic scattering data [16–19] consistently with $B(E2)$ of mirror transitions of ^{18}Ne and ^{18}O [20].

In study of unstable nuclei, the neutron collectivity, i.e., the M_n/M_p ratio has been investigated ex-

tensively with the inelastic proton scattering experiments in inverse kinematics using radioactive ion beam [3, 7, 9, 12, 21–32]. However, the reaction analysis still contains model ambiguities, for instance, in the proton-nucleus optical potentials, which are phenomenologically adjusted usually to elastic scattering cross sections but the applicability has not been well tested for inelastic scattering off exotic nuclei.

Recently, triggered by the complete microscopic folding model calculation by the Melbourne group [33, 34], the microscopic description of proton-nucleus [35–38] and α -nucleus [37, 39] elastic scattering, without any free adjustable parameter and phenomenological parametrization, has been developed. Very recently, the framework was successfully applied to α -nucleus inelastic processes [38, 40–42]. One of the advantages of this approach is that, once reliable densities of target nuclei are given, there is no adjustable parameter in the reaction part. As for the structure part, proton and neutron matter and transition densities are obtained by microscopic structure model calculations, which describe characteristics of nuclear properties such as the cluster, deformation, and neutron skin structures in target nuclei.

In this paper, we investigate the inelastic proton scattering to the 2_1^+ states of ^{18}O , ^{10}Be , ^{12}Be , and ^{16}C with the coupled-channel (CC) calculations of the microscopic single-folding model using the Melbourne g -matrix effective NN interaction [33]. The proton and neutron matter and transition densities of the target nuclei are calculated with antisymmetrized molecular dynamics (AMD) [43–45]. As test cases, we first show application to the proton scattering off $Z = N$ nuclei, ^{12}C and ^{16}O . Then, we apply the same method to the proton scattering off ^{18}O , ^{10}Be , ^{12}Be , and ^{16}C . The sensitivity of the 2_1^+ cross sections to M_n and M_p is analyzed while focusing on the neutron-proton difference in the transition densities in ^{12}Be and ^{16}C .

The paper is organized as follows. The next section describes the present framework of the microscopic coupled-channel (MCC) calculation and that of the structure calculations for target nuclei. Results of ^{12}C and ^{16}O are shown in Sec. III, and results and discussions for the $N \neq Z$ case of ^{18}O , ^{10}Be , ^{12}Be , and ^{16}C are given in Sec. IV. Finally, a summary is given in Sec. V.

II. METHOD

The present reaction calculation for the proton scattering is the MCC calculation of the single-folding model. As inputs from the structure calculations, the target densities are calculated with AMD combined with and without the cluster model of the generator coordinate method (GCM). The AMD and AMD+GCM calculations of target nuclei are the same as those of Refs. [4, 41, 42, 46–48]. The definitions of densities and form factors in the structure calculation are explained in Ref. [41]. For details, the reader is referred to those references.

A. Microscopic coupled-channel calculation

The diagonal and coupling potentials for the nucleon-nucleus system are microscopically calculated by folding the Melbourne g -matrix NN interaction [33] with the target densities described in Sec. II B. The Melbourne g matrix is obtained by solving a Bethe-Goldstone equation in a uniform nuclear matter at given incident energy; the Bonn-B potential [49] is adopted as a bare NN interaction. In Ref. [33], the Melbourne g -matrix interaction was constructed and applied to a systematic investigation on proton elastic and inelastic scattering off various stable nuclei and some neutron-rich nuclei at energies from 40 MeV to 300 MeV. The nonlocality coming from the exchange term was rigorously treated and the central, spin-orbit, and tensor contributions were taken into account. As a result, it was clearly shown that the microscopic calculation with the Melbourne g matrix for the proton-nucleus scattering has predictive power for the proton-nucleus elastic and inelastic cross sections and spin observables. Later, the framework was applied also to proton inelastic scattering off ^{10}C and ^{18}O [34].

In the present study, we adopt a simplified single-folding model described in Ref. [35]. We employ the Brieva and Rook (BR) prescription [50–52] to localize the exchange terms. The validity of the BR localization for nucleon-nucleus scattering was confirmed in Refs. [35, 53] and for nucleus-nucleus scattering in Ref. [54]. This simplified single-folding model has successfully been applied to nucleon-nucleus elastic scattering for various cases [35–38]. In this study, we extend the model to proton inelastic scattering in a similar manner to in our recent studies on α inelastic scattering [41, 42]. To avoid complexity, we take into account only the central part of the proton-nucleus potential. The spin-orbit interaction is

known to smear the dip structure of the diffraction pattern in general. Although at higher energies, say, above 150–200 MeV, it can somewhat affect the absolute amplitudes also near the peaks, such effect is expected to be minor in the energy region considered in this study. As in the previous studies including that by the Melbourne group [33], the local density approximation is adopted to apply the g -matrix interaction to a finite nucleus.

The cross sections of the elastic and inelastic scattering are calculated by the CC calculations using the proton-nucleus potentials obtained with the AMD densities for ^{18}O , ^{10}Be , ^{12}Be , and ^{16}C , and the AMD+GCM densities for ^{12}C and ^{16}O . For ^{12}C , we also use the densities of a 3α -cluster model of the resonating group method (RGM) [55].

It should be commented that a similar approach of the MCC calculation with the Jeukenne-Lejeune-Mahaux (JLM) interaction [56] has been applied to the proton inelastic scattering off ^{10}Be and ^{12}Be in the earlier work by Takashina *et al.* [11]. It was used also in continuum-discretized coupled-channels calculation for nucleon-induced breakup reactions of $^{6,7}\text{Li}$ [57–59] and ^{11}Li [60]. The JLM interaction is another kind of the g -matrix effective interaction that has only the direct term. This property allows one to implement it to reaction calculation with the minimal task. On the other hand, in general, phenomenological tuning of the JLM interaction is necessary to fit the scattering data.

B. Structure calculations for target nuclei

For the structure calculation of the target nuclei, we adopt the AMD wave functions obtained by the variation after projections (VAP). In the AMD+VAP method, the variation is performed for the spin-parity projected AMD wave function as done in Refs. [61, 62]. The method was applied for the structure studies of ^{10}Be , ^{12}Be , and ^{16}C in Refs. [4, 46, 47]. In the present paper, the same method is applied to ^{18}O to obtain the wave functions of the 0_1^+ and 2_1^+ states. For ^{12}C and ^{16}O , the AMD+VAP method is combined with the 3α - and $^{12}\text{C} + \alpha$ -cluster GCM, respectively, as done in Refs. [41, 42, 48, 63, 64]. In this paper, we simply call the AMD+VAP “AMD” and that with the cluster GCM “AMD+GCM”.

The AMD wave functions used in this paper are in principle the same as those of Refs. [47, 61]. We utilize the ^{10}Be wave function for ^{10}C by assuming the mirror symmetry. For ^{16}C , the VAP(c) wave function of Ref. [4] is adopted. The wave functions and transition densities of ^{12}C and ^{16}O are consistent with those of AMD+GCM used for the α scattering in Refs. [41, 42].

The neutron and proton matter and transition densities are calculated with the AMD and AMD+GCM wave functions. We denote the neutron and proton transition densities as $\rho_n^{\text{tr}}(r)$ and $\rho_p^{\text{tr}}(r)$, respectively. For $N = Z$ nuclei (^{12}C and ^{16}O), half of isoscalar density is used as the proton (neutron) density in the mirror symme-

try assumption. For quantitative discussions of inelastic cross sections, we scale the original transition densities $\rho_p^{\text{tr-cal}}(r)$ to adjust the theoretical $B(E\lambda)$ values to the experimental data as

$$\rho_p^{\text{tr}}(r) = (M_p^{\text{exp}}/M_p^{\text{cal}})\rho_p^{\text{tr-cal}}(r) \quad (1)$$

Here the rank λ ($\lambda > 0$) transition matrix elements for the neutron and proton parts are defined as

$$M_{n,p} \equiv \int r^{2+\lambda} \rho_{n,p}^{\text{tr}}(r) dr \quad (2)$$

and related to the transition strengths as

$$B_\lambda^{(n),(p)} = \frac{1}{2J_i + 1} |M_{n,p}|^2, \quad (3)$$

where J_i is the angular momentum of the initial state. The $E2$ transition strength is given by the proton $\lambda = 2$ transition strength as $B(E2) = e^2 B_{\lambda=2}^{(p)}$.

The adopted states in the CC calculation for ^{10}Be , ^{12}Be , ^{16}C , and ^{18}O are $^{10}\text{Be}(0_{1,2}^+, 2_{1,2,3}^+)$, $^{12}\text{Be}(0_{1,2}^+, 2_{1,2}^+)$, $^{16}\text{C}(0_1^+, 2_{1,2}^+)$, and $^{18}\text{O}(0_1^+, 2_1^+)$. All $\lambda = 0$ and $\lambda = 2$ transitions between these states are taken into account. The experimental values of excitation energies are adopted as inputs of the CC calculation.

In the CC calculations for ^{12}C and ^{16}O , all the inputs from the structure part such as the adopted states, excitation energies, and transitions are the same as those used for the α scattering with the AMD+GCM wave functions in Refs. [41, 42].

As shown later, the CC effect gives only minor contribution to the inelastic scattering to the 2_1^+ state at incident energies higher than 25 MeV, and the cross sections are approximately described by the one-step process of the distorted wave Born approximation (DWBA).

III. RESULTS OF ^{12}C AND ^{16}O

The 0_1^+ and 2_1^+ cross sections of ^{12}C at incident energies $E_p = 35, 65,$ and 135 MeV are shown in Fig. 1, and those of ^{16}O at $E_p = 35$ and 135 MeV are shown in Fig. 2. In addition to the CC calculation, the one-step cross sections obtained by the DWBA calculation are also shown. The small difference between the CC and DWBA cross sections indicates that the CC effect is minor.

The AMD+GCM result of ^{12}C is compared with experimental data and also with the calculation with the RGM density. From the electron scattering data, the RGM density is known to be good in quality and better than the AMD+GCM density [41, 55]. As seen in Fig. 1, the present calculation with the AMD+GCM density reproduces well the elastic proton scattering cross sections of ^{12}C at forward angles, but somewhat underestimates the third peak. A better result is obtained by the calculation with the RGM density, consistently with Ref. [38]. The inelastic proton scattering cross sections of $^{12}\text{C}(2_1^+)$ are described reasonably well with the

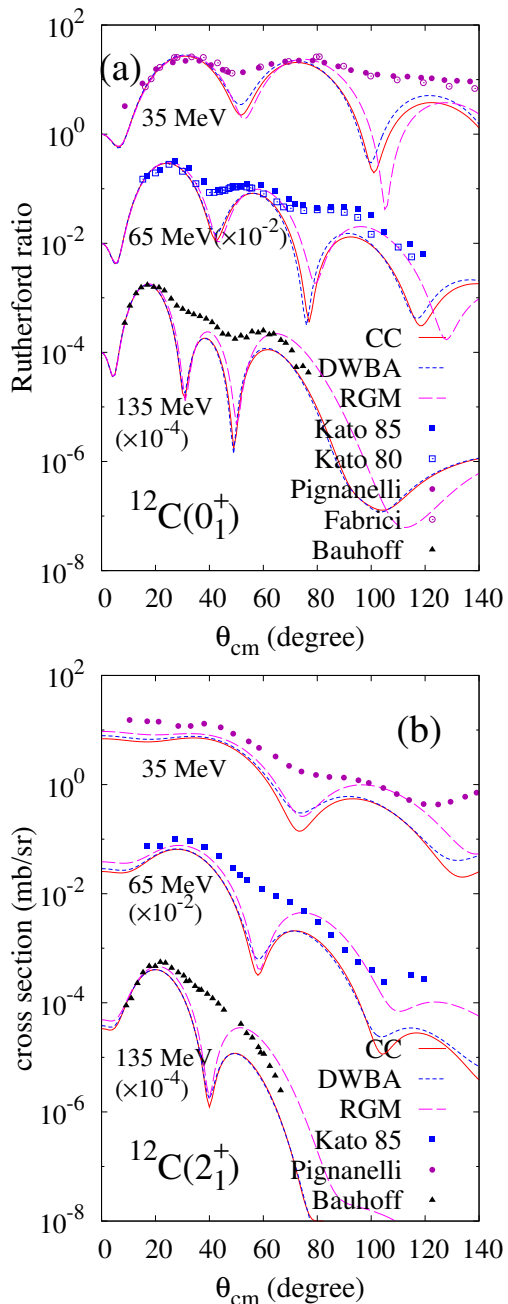


FIG. 1: Cross sections of the elastic and inelastic proton scattering off ^{12}C at $E_p = 35$ MeV, $E_p = 65$ MeV ($\times 10^{-2}$), and $E_p = 135$ MeV ($\times 10^{-4}$) calculated with the AMG+GCM and RGM densities. The results of the CC and DWBA calculations with the AMD+GCM densities and the CC calculation with the RGM densities are shown by red solid, blue dotted, and magenta dashed lines, respectively. The experimental data are from Refs. [65–69].

AMD+GCM and RGM calculations except for the cross sections at $E_p = 35$ MeV. The RGM density again gives a better agreement with the data at large angles. This result indicates that quality of the structure model den-

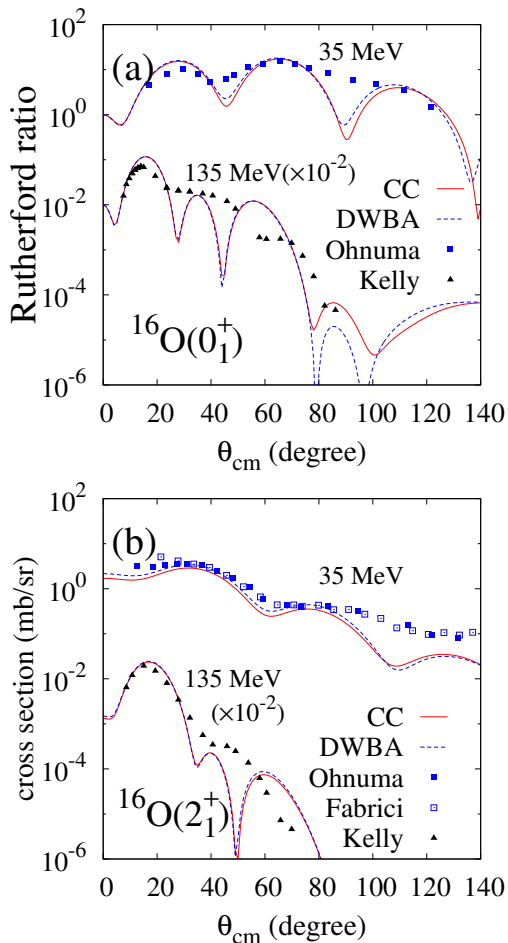


FIG. 2: Cross sections of the elastic and inelastic proton scattering off ^{16}O at $E_p = 35$ MeV and $E_p = 135$ MeV ($\times 10^{-2}$) calculated with the AMG+GCM densities. The results of the CC and DWBA calculations are shown by red solid and blue dotted lines, respectively. The experimental data are from Refs. [65, 70, 71].

sities can be tested by the detailed data of the proton scattering. For the proton scattering off ^{16}O , the present calculation reproduces well the elastic and inelastic cross sections (Fig. 2). It should be commented that the 2_1^+ state of ^{16}O is not the ground-band member but belongs to the $^{12}\text{C}+\alpha$ -cluster band built on the 0_2^+ state. The present microscopic approach works well even for such the developed cluster state with structure much different from the ground state.

IV. RESULTS OF $Z \neq N$ NUCLEI

A. Structure properties

The theoretical and experimental values of structure properties of the target nuclei are listed in Tables I and

II. The energies are shown in Table I, and radii and $\lambda = 2$ transition strengths as well as the M_n/M_p ratio are shown in Table II. The structure calculation of ^{10}Be , ^{12}Be , and ^{16}C are consistent with Refs. [4, 46, 47]. We will describe detailed properties of the 0_1^+ and 2_1^+ states and the transition between them later.

TABLE I: Binding and excitation energies of ^{18}O , ^{10}Be , ^{12}Be , and ^{16}C . Theoretical values of ^{10}Be , ^{12}Be , and ^{16}C are taken from Refs. [4, 46, 47], and experimental values are from Refs. [72–75]. The band assignment (K^π) are given based on the AMD calculation.

		Energy (MeV)	
		Band	AMD exp
$^{18}\text{O}(0_1^+)$	$K = 0_1^+$	131.1	139.80
$^{18}\text{O}(2_1^+)$	$K = 0_1^+$	2.0	1.98
$^{10}\text{Be}(0_1^+)$	$K = 0_1^+$	61.1	64.98
$^{10}\text{Be}(2_1^+)$	$K = 0_1^+$	2.7	3.37
$^{10}\text{Be}(2_2^+)$	$K = 2^+$	6.8	5.96
$^{10}\text{Be}(0_2^+)$	$K = 0_2^+$	7.8	6.179
$^{10}\text{Be}(2_3^+)$	$K = 0_2^+$	9.0	7.54
$^{12}\text{Be}(0_1^+)$	$K = 0_1^+$	61.9	68.65
$^{12}\text{Be}(2_1^+)$	$K = 0_1^+$	1.8	2.11
$^{12}\text{Be}(0_2^+)$	$K = 0_2^+$	3.6	2.251
$^{12}\text{Be}(2_2^+)$	$K = 0_2^+$	4.6	–
$^{16}\text{C}(0_1^+)$	$K = 0_1^+$	102.6	110.75
$^{16}\text{C}(2_1^+)$	$K = 0_1^+$	2.4	1.77
$^{16}\text{C}(2_2^+)$	$K = 2^+$	7.8	3.99

B. Results of ^{18}O

In the $2_1^+ \rightarrow 0_1^+$ transition of ^{18}O , the significant $B_{\lambda=2}^{(p)}$ has been experimentally known but it is much underestimated by the AMD calculation meaning that the proton excitation from the p -shell closure is not sufficiently described in the theory. For the neutron part, the large $B_{\lambda=2}^{(n)}$ of the AMD calculation indicates the neutron dominance, which is qualitatively consistent with the mirror transition of ^{18}Ne [20] and the proton scattering experiment [19].

The calculated densities and form factors of ^{18}O are shown in Figs. 3 and 4, respectively, together with the data measured by the electron scattering experiments. Here, the theoretical proton transition density $\rho_p^{\text{tr-cal}}(r)$ and form factors $F^{\text{cal}}(q)$ are scaled by the factor $M_p^{\text{exp}}/M_p^{\text{cal}} = 3.88$ as $\rho_p^{\text{tr}}(r) = (M_p^{\text{exp}}/M_p^{\text{cal}})\rho_p^{\text{tr-cal}}(r)$ and $F(q) = (M_p^{\text{exp}}/M_p^{\text{cal}})F^{\text{cal}}(q)$ so as to fit the experimental $B(E2)$ value. After the scaling, the experimental

TABLE II: Matter, proton, and neutron radii, and transition strengths of ^{18}O , ^{10}Be , ^{12}Be , and ^{16}C . Theoretical values of the AMD calculation for ^{10}Be , ^{12}Be , and ^{16}C are from Refs. [4, 46, 47], and experimental values are taken from Refs. [72–75]. The data of $B_{\lambda=2}^{(p)} = B(E2)/e^2$ for ^{16}C are the values reported in Refs. [13, 76]. * The experimental values of $B(E2)/e^2$ of the mirror nuclei (^{18}Ne and ^{10}C) are shown for $B_{\lambda=2}^{(n)}$ of ^{18}O and ^{10}Be .

	R_p (fm)	R_n (fm)	R_m (fm)
$^{18}\text{O}(0_1^+)$	2.75	2.88	2.82
exp	2.62	2.83 ^{*mir}	2.61(8)
	$B_{\lambda=2}^{(p)}$ (fm ⁴)	$B_{\lambda=2}^{(n)}$ (fm ⁴)	M_n/M_p
$^{18}\text{O}(2_1^+ \rightarrow 0_1^+)$	0.7	18.6	5.4
exp	9.3(3)	50(5) ^{*mir}	2.3(2) ^{*mir}
	R_p (fm)	R_n (fm)	R_m (fm)
$^{10}\text{Be}(0_1^+)$	2.50	2.56	2.54
exp	2.17		2.30(2)
	$B_{\lambda=2}^{(p)}$ (fm ⁴)	$B_{\lambda=2}^{(n)}$ (fm ⁴)	M_n/M_p
$^{10}\text{Be}(2_1^+ \rightarrow 0_1^+)$	11.6	8.9	0.9
exp	10.2(1.0)	12.2(1.9) ^{*mir}	1.1(1) ^{*mir}
$^{10}\text{Be}(2_2^+ \rightarrow 0_1^+)$	0.2	3.2	3.9
$^{10}\text{Be}(2_3^+ \rightarrow 0_1^+)$	0.1	0.7	2.5
$^{10}\text{Be}(2_3^+ \rightarrow 0_2^+)$	34.5	118	1.8
	R_p (fm)	R_n (fm)	R_m (fm)
$^{12}\text{Be}(0_1^+)$	2.67	2.94	2.85
exp	2.39		2.59(6)
$^{12}\text{Be}(0_2^+)$	2.56	2.84	2.75
	$B_{\lambda=2}^{(p)}$ (fm ⁴)	$B_{\lambda=2}^{(n)}$ (fm ⁴)	M_n/M_p
$^{12}\text{Be}(2_1^+ \rightarrow 0_1^+)$	14.4	51.1	1.9
exp	14.2(2.8)		
$^{12}\text{Be}(2_2^+ \rightarrow 0_1^+)$	0.0	7.4	25.4
$^{12}\text{Be}(2_2^+ \rightarrow 0_2^+)$	7.5	9.0	1.1
	R_p (fm)	R_n (fm)	R_m (fm)
$^{16}\text{C}(0_1^+)$	2.58	2.85	2.75
exp			2.70(3)
	$B_{\lambda=2}^{(p)}$ (fm ⁴)	$B_{\lambda=2}^{(n)}$ (fm ⁴)	M_n/M_p
$^{16}\text{C}(2_1^+ \rightarrow 0_1^+)$	2.7	27.0	3.2
exp [76]	2.6(9)		
exp [13]	4.15(73)		
$^{16}\text{C}(2_2^+ \rightarrow 0_1^+)$	2.6	0.1	0.2

data are reproduced well except for the small r (large q) region.

For the neutron transition density $\rho_n^{\text{tr}}(r)$ of ^{18}O , we tentatively assume the mirror symmetry and scale $\rho_n^{\text{tr-cal}}(r)$ with the scaling factor $M_p^{\text{exp}}(^{18}\text{Ne})/M_n^{\text{cal}} = 1.72$ to prepare the default input $\rho_n^{\text{tr}}(r)$ in the reaction calculation. However, if we take into account the mirror symmetry breaking, another choice may be possible, for example, about a 10% smaller value than $M_p^{\text{exp}}(^{18}\text{Ne})$ was theoretically recommended for $M_n(^{18}\text{O})$ in Ref. [19].

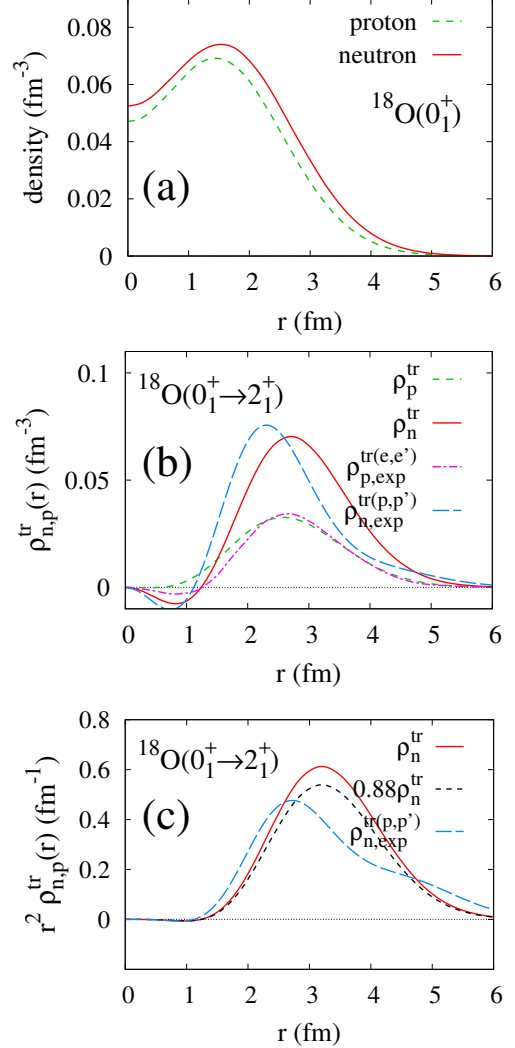


FIG. 3: Neutron and proton densities of ^{18}O . (a) The neutron and proton matter densities of the ground state, (b) the neutron and proton transition densities for the $0_1^+ \rightarrow 2_1^+$ transition, and (c) the r^2 -weighted neutron transition density calculated with AMD. The renormalized proton and neutron transition densities adjusted to the experimental $B(E2)$ of ^{18}O and that of ^{18}Ne are shown, respectively. The experimental neutron transition density $\rho_{n,\text{exp}}^{\text{tr}(p,p')}$ reduced from the (p,p') scattering at $E = 135$ MeV/u [19] and the experimental proton transition density $\rho_{p,\text{exp}}^{\text{tr}(e,e')}$ measured with the electron scattering data [77] are also shown.

In Figs. 3(b) and (c), the default $\rho_n^{\text{tr}}(r)$ is compared with the experimental estimation (denoted by $\rho_{n,\text{exp}}^{\text{tr}(p,p')}$) of Ref. [19], which was reduced from the inelastic proton scattering at $E = 135$ MeV/u by a model analysis. $\rho_{n,\text{exp}}^{\text{tr}(p,p')}$ gives $B_{\lambda=2}^{(n)} = 38$ fm⁴, which is slightly smaller than $B_{\lambda=2}^{(n)} = 50$ fm⁴ of $\rho_n^{\text{tr}}(r)$ adjusted to $B(E2;^{18}\text{Ne})$. The 12% reduced transition density ($0.88\rho_n^{\text{tr}}(r)$) gives the same strengths ($B_{\lambda=2}^{(n)} = 38$ fm⁴) as $\rho_{n,\text{exp}}^{\text{tr}(p,p')}$, but it

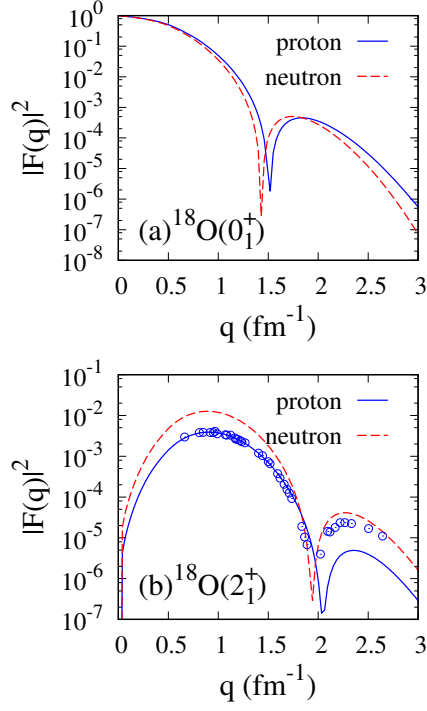


FIG. 4: Elastic and inelastic form factors of ^{18}O . The inelastic form factors for $0_1^+ \rightarrow 2_1^+$ are the renormalized ones adjusted to experimental $B(E\lambda)$. The experimental data measured by the electron scattering are from Ref. [77].

shows a different radial behavior from $\rho_{n,\text{exp}}^{\text{tr}(p,p')}(r)$. Compared with the theoretical transition density, $\rho_{n,\text{exp}}^{\text{tr}(p,p')}(r)$ has the smaller amplitude at the nuclear surface ($r = 3\text{--}4$ fm) and enhanced outer tail in $r \gtrsim 5$ fm region (see Fig. 3(c)). In the reaction analysis, we consider this difference between $\rho_{n,\text{exp}}^{\text{tr}(p,p')}(r)$ and the default $\rho_n^{\text{tr}}(r)$ as a model ambiguity from the neutron transition density.

We calculate the cross sections of the proton scattering at $E = 24.5$ MeV/u, 35 MeV/u, 43 MeV/u, and 135 MeV/u, and those of the neutron scattering at $E = 24$ MeV/u. They are compared with the experimental data. The results are shown in Figs. 5 and 6. The calculation reproduces reasonably well the elastic and inelastic proton scattering cross sections in the wide range of $E = 24\text{--}135$ MeV/u. It also reproduces well the neutron scattering cross sections at $E = 24$ MeV/u. In comparison with the DWBA calculation shown in Fig. 7, one can see that the CC effect is minor in the 2_1^+ cross sections.

Let us discuss the ambiguity from the proton and neutron transition densities. As shown previously, the (scaled) proton part $\rho_p^{\text{tr}}(r)$ used in the present calculation reproduces well the experimental data measured by the electron scattering, whereas the neutron part $\rho_n^{\text{tr}}(r)$ has the r behavior different from the experimental one $\rho_{n,\text{exp}}^{\text{tr}(p,p')}(r)$. In order to see the effect of this difference in the neutron transition density to the inelastic cross

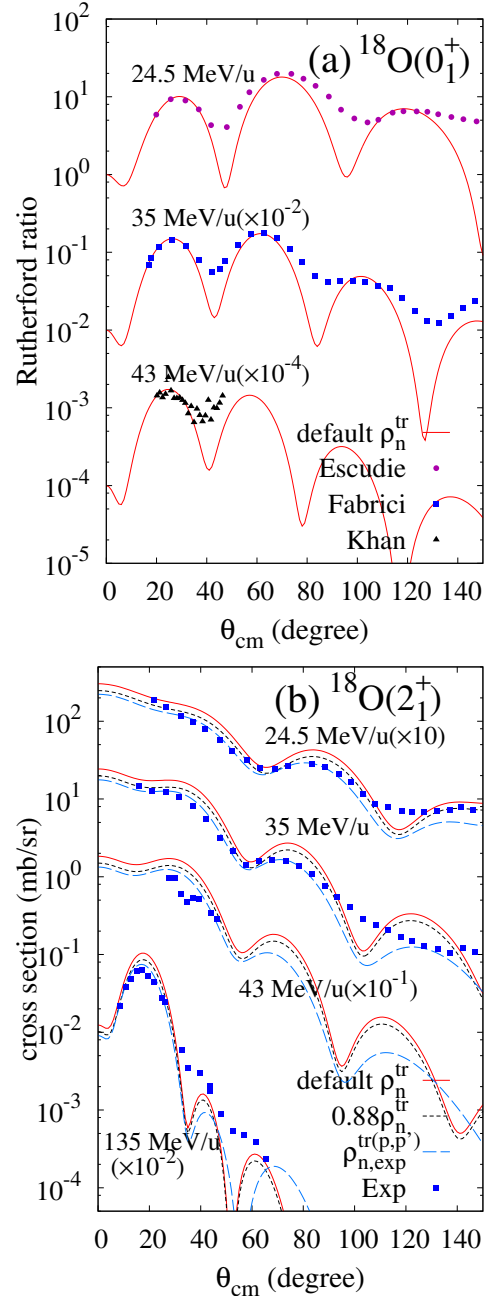


FIG. 5: Cross sections of the elastic and inelastic proton scattering off ^{18}O at $E = 24$ MeV/u ($\times 10$), 35 MeV/u, 43 MeV/u ($\times 10^{-1}$), and 135 MeV/u ($\times 10^{-2}$) calculated with the default AMD densities (solid lines). The experimental data for $E = 43$ MeV/u are the cross sections measured in inverse kinematics. For the 2_1^+ cross sections, the calculated result with the experimental neutron transition density $\rho_{n,\text{exp}}^{\text{tr}(p,p')}(r)$ and that with the reduced neutron transition density $0.88\rho_n^{\text{tr}}(r)$ are also shown by dashed and dotted lines, respectively. The experimental data are from Refs. [19, 21, 65, 78]

sections, we perform the same reaction calculation using $\rho_{n,\text{exp}}^{\text{tr}(p,p')}(r)$ and $0.88\rho_n^{\text{tr}}(r)$. Figures 5(b) and 6(b) show

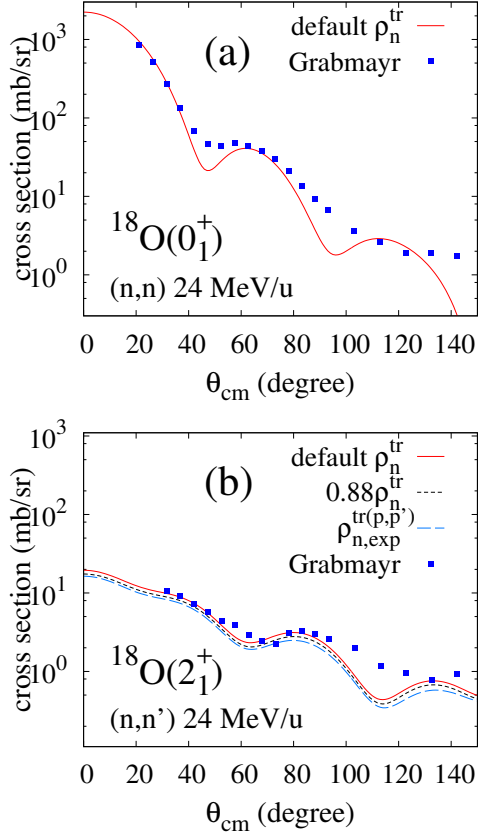


FIG. 6: Cross sections of (a) elastic and (b) inelastic neutron scattering off ^{18}O at $E = 24$ MeV/u. For the 2_1^+ cross sections, the CC calculation with the experimental neutron transition density $\rho_{n,\text{exp}}^{\text{tr}(p,p')}(r)$ and that with $0.88\rho_n^{\text{tr}}(r)$ are also shown by blue dotted and light-blue dashed lines, respectively, in addition to that with the default AMD densities (red solid lines). The data are from Ref. [18].

respectively the proton and neutron scattering cross sections obtained with $\rho_{n,\text{exp}}^{\text{tr}(p,p')}(r)$ (light blue dashed lines) and that with $0.88\rho_n^{\text{tr}}(r)$ (blue dotted lines) in comparison with the default calculation (red solid lines) and experimental data. In the result of the proton scattering with $\rho_{n,\text{exp}}^{\text{tr}(p,p')}(r)$, the cross sections at forward angle slightly decrease to 70% of the default calculation, and the second and third peaks at the large angles are reduced further to 40–60% of the default calculation. The reduction rate at large angles is larger than the naive expectation of $38/50 \approx 75\%$ from the $B_{\lambda=2}^{(n)}$ ratio. It means that the outer tail amplitude of the neutron transition density gives relatively minor contribution to the proton scattering cross sections than the surface amplitude though it significantly enhances the M_n , i.e., $B_{\lambda=2}^{(n)}$. The calculation with $\rho_{n,\text{exp}}^{\text{tr}(p,p')}(r)$ obtains better agreement with the proton scattering data at least at $E = 24.5$ MeV/u and 35 MeV/u suggesting that $\rho_{n,\text{exp}}^{\text{tr}(p,p')}(r)$ may be favored

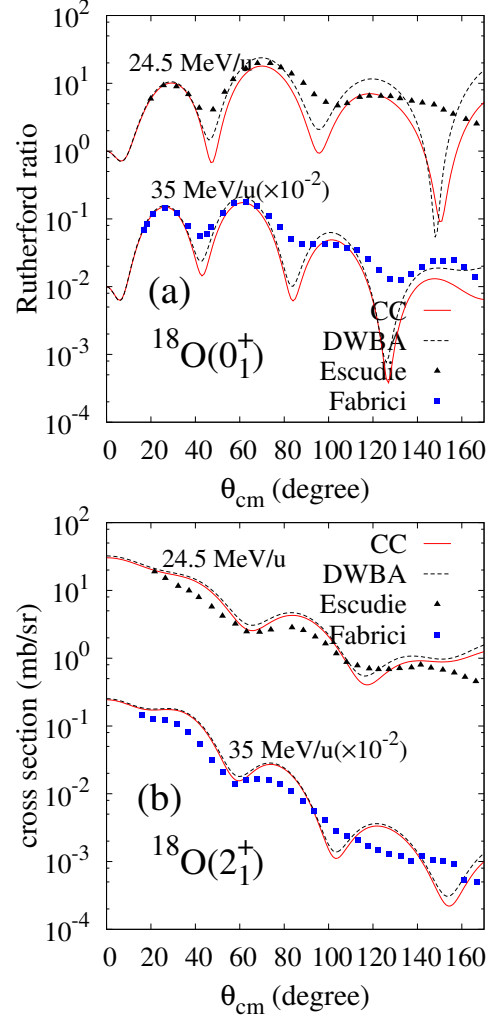


FIG. 7: Comparison of the CC and DWBA calculations of the proton scattering off ^{18}O with the default $\rho_n^{\text{tr}}(r)$. The (a) elastic and (b) inelastic cross sections at $E = 24.5$ MeV/u and 35 MeV/u are shown in comparison with the experimental data [65, 78].

rather than the default $\rho_n^{\text{tr}}(r)$ used in the present calculation. It indicates that the proton scattering is a sensitive probe for the neutron transition density. In contrast to the proton scattering, the neutron scattering cross sections are not so sensitive to the difference in the neutron transition densities as expected from the weaker nn interactions than the pn ones.

C. Results of ^{10}Be , ^{12}Be , and ^{16}C

The structure studies of ^{10}Be , ^{12}Be , and ^{16}C with AMD have been done in Refs. [4, 46, 47]. We here briefly describe the structure properties, in particular, of the ground bands in these nuclei.

In ^{10}Be , the $M_n/M_p = 0.9$ of the ground-band tran-

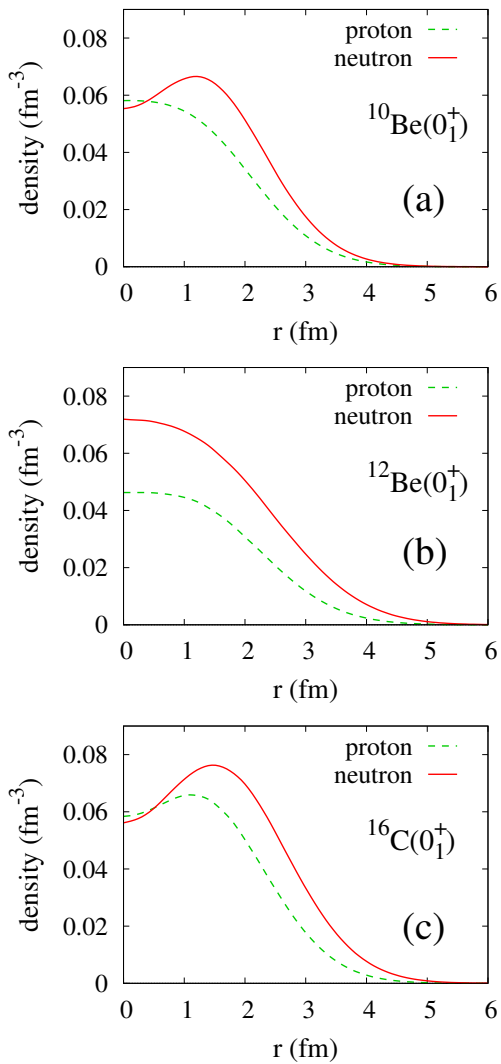


FIG. 8: Neutron and proton matter densities of the ground states of (a) ^{10}Be , (b) ^{12}Be , and (c) ^{16}C calculated with AMD.

sition $2_1^+ \rightarrow 0_1^+$ in the AMD calculation is smaller than $N/Z = 1.5$ naively expected from the collective model and in reasonable agreement with the experimental value ($M_n/M_p = 1.1$) reduced from $B(E2)$ of mirror transitions. It indicates that the neutron excitation is somewhat suppressed compared with the proton excitation in the 2_1^+ state. In addition to the 2_1^+ state of the ground $K^\pi = 0^+$ band, the 2_2^+ state of the side band ($K^\pi = 2^+$) is obtained because of the triaxial deformation. In the higher energy region, the second $K^\pi = 0^+$ band with the developed cluster structure appears.

In ^{12}Be , the breaking of $N = 8$ magicity is known in the ground state from various experimental observations such as the Gamov-Tellar transitions, inelastic scattering, and knock-out reactions [3, 82–86]. The AMD calculation obtains the largely deformed ground band ($K^\pi = 0_1^+$) with the dominant neutron $2\hbar\omega$ component. The ground-band

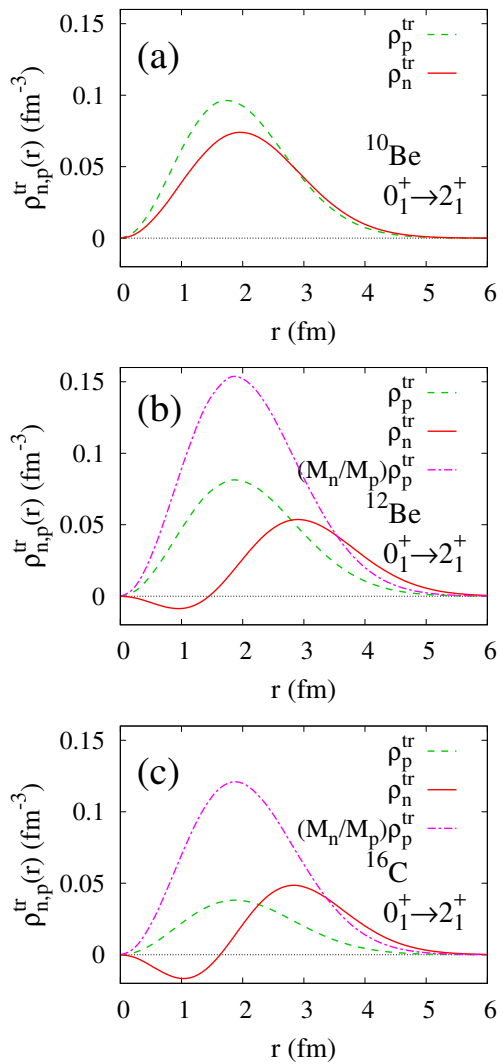


FIG. 9: Neutron (ρ_n^{tr}) and proton (ρ_p^{tr}) transition densities for $0_1^+ \rightarrow 2_1^+$ of (a) ^{10}Be , (b) ^{12}Be , and (c) ^{16}C calculated with AMD. The proton and neutron transition densities of ^{10}Be are renormalized to adjust the experimental $B(E2)$ value of ^{10}Be and that of ^{10}C , respectively.

transition, $2_1^+ \rightarrow 0_1^+$, is strong because of the large deformation compared with the weaker transition in the $K^\pi = 0_2^+$ band, which corresponds to the normal neutron p -shell closed configuration. In particular, the neutron transition is considerably strong because of the contribution of two sd -orbit neutrons. The values of the ratio $M_n/M_p = 1.9$ ($M_n/M_p = 1.1$) is obtained for the $K^\pi = 0_1^+$ ($K^\pi = 0_2^+$) band. The ratio of the ground band is as large as $N/Z = 2$ because of the breaking of the $N = 8$ magicity.

In the case of ^{16}C , the AMD calculation predicted the weak proton transition in $2_1^+ \rightarrow 0_1^+$ because of the $Z = 6$ sub-shell closure. The observed $B(E2)$ values are consistent with the prediction. On the other hand, the neutron transition is significantly large because of the contribu-

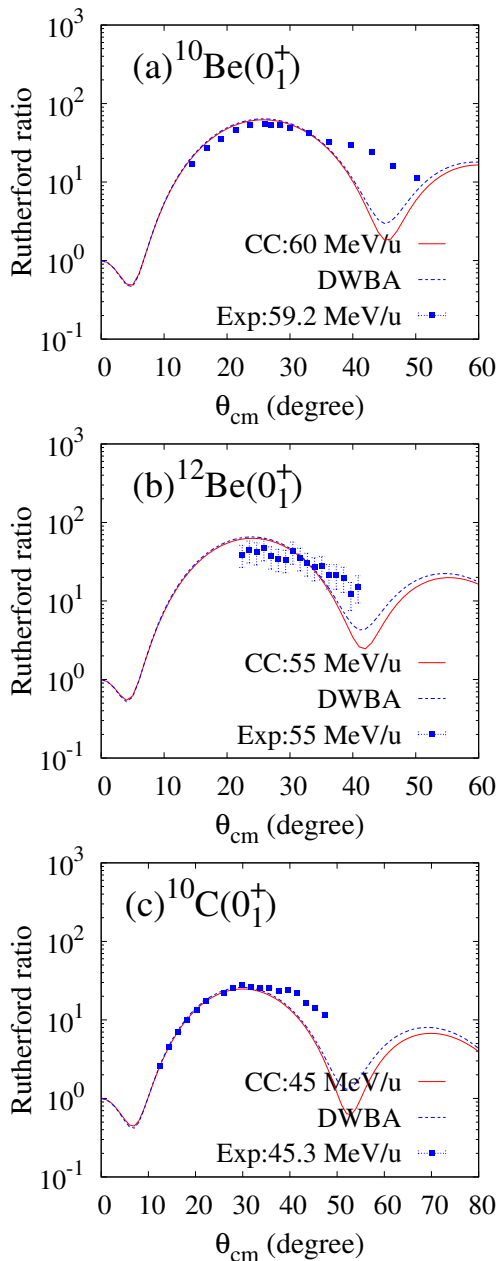


FIG. 10: Cross sections of the elastic proton scattering off (a) ^{10}Be at $E = 60$ MeV/u, (b) ^{12}Be at $E = 55$ MeV/u, and (c) ^{10}C at $E = 45$ MeV/u calculated by the CC calculation with the AMD densities (red solid lines). The one-step cross sections obtained by the DWBA calculation are also shown (blue dotted lines). The calculations are compared with the experimental data measured in inverse kinematics of ^{10}Be at 59.2 MeV/u[79], ^{12}Be at 55 MeV/u[80], and ^{10}C at 45.3 MeV/u[7].

tion of the sd -orbit neutrons, and results in the much larger ratio $M_n/M_p = 3.2$ than $N/Z = 1.67$, i.e., the dominant neutron contribution in the ground-band transition.

Figure 9 shows the neutron and proton matter densities of the ground state and the neutron and proton transition densities of the $2_1^+ \rightarrow 0_1^+$ transition of ^{10}Be , ^{12}Be , and ^{16}C . In ^{10}Be , the proton and neutron transition densities have the peak amplitude at the same position at the nuclear surface and approximately satisfy the relation $\rho_n^{\text{tr}}(r) = (M_n/M_p)\rho_p^{\text{tr}}(r)$. By contrast, in ^{12}Be and ^{16}C , the neutron transition density shows the r behavior quite different from the proton transition density. It has the peak amplitude in $r \approx 3$ fm region much outer than the proton transition density because of the contribution of the sd -orbit neutrons and no longer satisfies the relation $\rho_n^{\text{tr}}(r) = (M_n/M_p)\rho_p^{\text{tr}}(r)$. This is a different feature from ^{10}Be , where the protons and neutrons in the same p shell contribute to the 2_1^+ excitation.

The proton scattering cross sections are calculated with the AMD densities. For ^{10}Be , the theoretical proton and neutron transition densities are renormalized to fit the experimental transition strengths ($B_{\lambda=2}^{(p),(n)}$) by the scaling factors $M_{p,n}^{\text{exp}}/M_{p,n}^{\text{cal}}$ listed in Table II. For ^{12}Be and ^{16}C , we use the original AMD transition densities, which reproduce well the experimental $B(E2)$ values. The calculated elastic and inelastic cross sections of ^{10}Be at $E = 60$ MeV/u, ^{12}Be at $E = 55$ MeV/u, and ^{10}C at $E = 45$ MeV/u are shown in Figs. 10 and 11. They are compared with the experimental data measured in inverse kinematics. In Fig. 12, the calculated cross sections of ^{16}C at $E = 33$ MeV/u are compared with the experimental data. The present calculation reproduces well the absolute amplitude of the 2_1^+ cross sections as well as the elastic cross sections.

In Fig. 9(b) for ^{12}Be , the DWBA calculation with the neutron transition density $\rho_n^{\text{tr}}(r) = (M_n/M_p)\rho_p^{\text{tr}}(r)$ is also shown. This calculation corresponds to the case with the collective model transition density. Compared with the result using the original AMD transition density, the cross sections somewhat increase and the peak and dip positions slightly shift toward larger angles.

For the neutron transition in ^{12}Be and ^{16}C , there is no data from the mirror nuclei. The good reproduction of the inelastic cross sections supports reliability of the neutron transition densities adopted in the present calculation, that is, the dominant neutron contributions as $M_n/M_p \approx 2$ and $M_n/M_p \approx 3$ for ^{12}Be and ^{16}C , respectively. This result is qualitatively consistent with those in Refs. [9, 11]. It should be stressed again that phenomenological adjustable parameters were needed in the reaction models of Refs. [9, 11], but not in the present model. For further detailed discussion of the transition densities, higher quality data are required.

D. Discussions

We discuss how one can link the inelastic proton scattering cross sections with the neutron transition matrix element M_n of the $0_1^+ \rightarrow 2_1^+$ transition. The experimental studies of Refs. [3, 9] have discussed the neutron matrix

elements of ^{12}Be and ^{16}C with the reaction analysis of the proton scattering data, and concluded the significant neutron contribution in the $0_1^+ \rightarrow 2_1^+$ transition. According to the model analysis in Refs. [3, 9] using the Bernstein prescription [1], $B_{\lambda=2}^{(n)} = 17 \text{ fm}^4$ of ^{12}Be is obtained by the reaction analysis using $B(E2) = 14.2(2.8) e^2 \text{ fm}^4$, and $B_{\lambda=2}^{(n)} = 25 \text{ fm}^4$ of ^{16}C is reduced using the updated data of $B(E2) = 2.6(9) e^2 \text{ fm}^4$ [9]. The value of ^{16}C is consistent with our value of $B_{\lambda=2}^{(n)} = 27.0 \text{ fm}^4$, but the value of ^{12}Be is much smaller than $B_{\lambda=2}^{(n)} = 51.1 \text{ fm}^4$ of the present calculation. In the theoretical study of the proton scattering of ^{12}Be with a MCC calculation using the same AMD densities [11], the slightly smaller value $B_{\lambda=2}^{(n)} = 37 \text{ fm}^4$ was favored to reproduce the inelastic cross sections.

The reaction analysis with the Bernstein prescription usually assumes the simple collective model transition densities given by the derivative of the matter density, and follows the relation of inelastic hadron (h, h') scattering cross sections with the transition matrix elements as

$$\sigma(h, h') \propto |b_n^{(h, h')} M_n + b_p^{(h, h')} M_p|^2, \quad (4)$$

where $b_n^{(h, h')}$ and $b_p^{(h, h')}$ are the neutron and proton field strengths of the external field from the hadron probe. For the proton scattering, $b_n^{(p, p')}/b_p^{(p, p')}$ depends on the energy. A standard value $b_n^{(p, p')}/b_p^{(p, p')} \approx 3$ at $E = 10\text{--}50 \text{ MeV/u}$, which was obtained from the data of various ordinary nuclei, is often used. The Bernstein prescription has been widely used for the inelastic proton scattering, but it greatly relies on the reaction model, which contains ambiguity such as the proton-nucleus optical potentials and the transition densities. The ansatz of Eq. (4) means the linear relation of the squared cross section with the neutron (M_n) and proton (M_p) transition matrix elements. The ratio $b_n^{(p, p')}/b_p^{(p, p')}$ indicates the sensitivity of the cross sections to the neutron transition matrix element (M_n) relative to the proton part (M_p), and is supposed to be system independent. The linear relation could be valid only if the relation $\rho_n^{\text{tr}}(r) \propto \rho_p^{\text{tr}}(r)$ is satisfied.

However, it is not the case with ^{12}Be and ^{16}C , for which the neutron transition density has the outer amplitude than the proton part. Such the exotic behavior of the neutron transition density may give non-trivial effects on the relation between the cross sections and the transition matrix elements (M_n and M_p). To see this effect we microscopically derive the ratio $b_n^{(p, p')}/b_p^{(p, p')}$ within the present MCC approach and discuss how the sensitivity of the cross section to M_n changes depending on the system as well as on the incident energy.

Here we assume that the AMD calculation gives correct r dependence of the $\rho_n^{\text{tr}}(r)$ and $\rho_p^{\text{tr}}(r)$ but contains ambiguity of the overall factor in each of the neutron and proton parts. By artificially changing the overall factor of

$\rho_n^{\text{tr}}(r)$ or $\rho_p^{\text{tr}}(r)$, we calculate the integrated cross sections and reduce the coefficients in the relation

$$\sigma(p, p') = |a_n^{(p, p')}(^A Z, E) M_n + a_p^{(p, p')}(^A Z, E) M_p|^2. \quad (5)$$

Here $a_n^{(p, p')}$ and $a_p^{(p, p')}$ are the system- and energy-dependent parameters determined from the calculated cross sections. The ratio $a_n^{(p, p')}/a_p^{(p, p')}$ is nothing but the ratio $b_n^{(p, p')}/b_p^{(p, p')}$ to be discussed.

In Fig. 13, we show the obtained result of $b_n^{(p, p')}/b_p^{(p, p')} = a_n^{(p, p')}/a_p^{(p, p')}$ for each systems, ^{18}O , ^{10}Be , ^{12}Be , and ^{16}C , with the default transition densities by open squares, crosses, filled circles, and filled triangles, respectively. For ^{12}Be and ^{16}C , we also show the result for the naive case of $\rho_n^{\text{tr}}(r) \propto \rho_p^{\text{tr}}(r)$ by open circles and triangles, respectively, which are obtained by the MCC calculation using $\rho_n^{\text{tr}}(r) = (M_n/M_p)\rho_p^{\text{tr}}(r)$. In all the cases, the calculated values of $b_n^{(p, p')}/b_p^{(p, p')}$ show similar energy dependence, i.e., decreasing with the increase of E . This energy dependence mainly comes from the energy dependence of the effective g -matrix NN interactions. In fact, if the nucleon-nucleus optical potentials fixed at $E = 60 \text{ MeV/u}$ is used, $b_n^{(p, p')}/b_p^{(p, p')}$ varies slightly from 1.90 (1.64) to 1.89 (1.57) in the energy range 30–120 MeV/u for the proton scattering off ^{10}Be (^{12}Be).

At each energy, almost the same values of $b_n^{(p, p')}/b_p^{(p, p')}$ are obtained for ^{18}O and ^{10}Be , and also by the calculation with the $\rho_n^{\text{tr}}(r) = (M_n/M_p)\rho_p^{\text{tr}}(r)$ assumption for ^{12}Be and ^{16}C . These values can be regarded as standard values for ordinary systems with $\rho_n^{\text{tr}}(r) \approx (M_n/M_p)\rho_p^{\text{tr}}(r)$. However, in the exotic case $\rho_n^{\text{tr}}(r) \neq (M_n/M_p)\rho_p^{\text{tr}}(r)$ of ^{12}Be and ^{16}C with the default transition densities, the values of $b_n^{(p, p')}/b_p^{(p, p')}$ significantly deviate from the standard values: they are smaller than the standard values by about 0.3 indicating that the sensitivity of the cross sections to M_n is by about 15% weaker than the ordinary case of $\rho_n^{\text{tr}}(r) = (M_n/M_p)\rho_p^{\text{tr}}(r)$. The reason for the weaker sensitivity of the cross sections is that the outer amplitude of the neutron transition density significantly contributes to M_n but does not so much to the cross sections.

This result may suggest a possible modification of the phenomenological reaction analysis. For simplicity, let us suppose that there is no ambiguity in the reaction model except for the neutron transition density $\rho_n^{\text{tr}}(r)$, and other inputs are so reliable that the model can properly reproduce the cross sections for the ordinary case. If one performs an inconsistent analysis using $\rho_n^{\text{tr}}(r) = (M_n/M_p)\rho_p^{\text{tr}}(r)$ for the exotic case, one could draw an underestimated value of M_n from the observed cross sections.

V. SUMMARY

We investigated the proton inelastic scattering off ^{18}O , ^{10}Be , ^{12}Be , and ^{16}C to the 2_1^+ states with the micro-

scopic coupled-channel calculation. The proton-nucleus potentials are microscopically derived by folding the Melbourne g -matrix NN interaction with the AMD densities of the target nuclei. The calculated result reasonably reproduces the elastic and inelastic proton scattering cross sections, and supports the dominant neutron contribution in the 2_1^+ excitation of ^{12}Be and ^{16}C . In order to discuss the detailed behavior of transition densities, further high quality data of the differential cross sections are required.

The sensitivity of the inelastic scattering cross sections to the neutron transition density was discussed. A particular attention was paid on the exotic systems such as ^{12}Be and ^{16}C that the neutron transition density has the remarkable amplitude in the outer region than the proton part. This outer amplitude of the neutron transition density significantly contributes to the neutron matrix element M_n . However, its contribution to the inelastic cross sections is quite modest because the reaction process considered has no strong selectivity for the outer region. This result indicates that a phenomenological analysis with the Bernstein prescription is no longer valid. Our finding will suggest that a phenomenological analysis with collective model transition densities can result in an undershooting of M_n for such exotic systems.

Acknowledgments

The computational calculations of this work were performed by using the supercomputer in the Yukawa Institute for theoretical physics, Kyoto University. This work was partly supported by Grants-in-Aid of the Japan Society for the Promotion of Science (Grant Nos. JP18K03617, JP16K05352, and 18H05407) and by the grant for the RCNP joint research project.

Appendix A: Resummation factor in the folding model calculation

According to the multiple scattering theory for nucleon-nucleus scattering constructed by Kerman, McManus, and Thaler [87], the transition matrix T is given by

$$T = \frac{A}{A-1} T', \quad (\text{A1})$$

where A is the mass number of the nucleus and T' is the transition matrix corresponding to the Schrödinger equation

$$\left[K + h + \frac{A-1}{A} \sum_{j=1}^A \tau_j - E \right] \Psi = 0. \quad (\text{A2})$$

K is the kinetic energy operator, h is the internal Hamiltonian of the nucleus, E is the total energy, and Ψ is the total wave function. τ_j is the effective interaction between the incident nucleon and a nucleon inside the nucleus, which is approximated to the Melbourne g -matrix NN interaction in this study. The two factors, $A/(A-1)$ in Eq. (A1) and $(A-1)/A$ in Eq. (A2) appear as a result of the *resummation* of the NN collisions originally written in terms of a bare NN interaction. Although these resummation factors usually do not play a role, for nucleon scattering off a light nucleus especially at low energies, these may slightly modify the result as shown in Ref. [38]. These factors are taken into account in all the calculations shown in the present calculation.

-
- [1] A. M. Bernstein, V. R. Brown and V. A. Madsen, Phys. Lett. **103B**, 255 (1981).
 - [2] Y. Kanada-En'yo and H. Horiuchi, Phys. Rev. C **55**, 2860 (1997).
 - [3] H. Iwasaki *et al.*, Phys. Lett. B **481**, 7 (2000).
 - [4] Y. Kanada-En'yo, Phys. Rev. C **71**, 014310 (2005).
 - [5] Y. Kanada-En'yo, Phys. Rev. C **71**, 014303 (2005).
 - [6] H. Sagawa, X. R. Zhou, X. Z. Zhang and T. Suzuki, Phys. Rev. C **70**, 054316 (2004).
 - [7] C. Jouanne *et al.*, Phys. Rev. C **72**, 014308 (2005).
 - [8] M. Takashina, Y. Kanada-En'yo and Y. Sakuragi, Phys. Rev. C **71**, 054602 (2005).
 - [9] H. J. Ong *et al.*, Phys. Rev. C **73**, 024610 (2006).
 - [10] T. J. Burvenich, W. Greiner, L. Guo, P. Klupfel and P. G. Reinhard, J. Phys. G **35**, 025103 (2008).
 - [11] M. Takashina and Y. Kanada-En'yo, Phys. Rev. C **77**, 014604 (2008).
 - [12] Z. Elekes, N. Aoi, Z. Dombradi, Z. Fulop, T. Motobayashi and H. Sakurai, Phys. Rev. C **78**, 027301 (2008).
 - [13] M. Wiedeking *et al.*, Phys. Rev. Lett. **100**, 152501 (2008).
 - [14] J. M. Yao, J. Meng, P. Ring, Z. X. Li, Z. P. Li and K. Hagino, Phys. Rev. C **84**, 024306 (2011).
 - [15] C. Forssn, R. Roth and P. Navrtil, J. Phys. G **40**, 055105 (2013).
 - [16] A. M. Bernstein, V. R. Brown and V. A. Madsen, Phys. Lett. **71B**, 48 (1977).
 - [17] S. Iversen *et al.*, Phys. Rev. Lett. **40**, 17 (1978).
 - [18] P. Grabmayr, J. Rapaport and R. W. Finlay, Nucl. Phys. A **350**, 167 (1980).
 - [19] J. Kelly *et al.*, Phys. Lett. **169B**, 157 (1986).
 - [20] A. M. Bernstein, V. R. Brown and V. A. Madsen, Phys. Rev. Lett. **42**, 425 (1979).
 - [21] E. Khan *et al.*, Phys. Lett. B **490**, 45 (2000).
 - [22] J. K. Jewell *et al.*, Phys. Lett. B **454**, 181 (1999).
 - [23] E. Khan *et al.*, Nucl. Phys. A **694**, 103 (2001).
 - [24] H. Scheit *et al.*, Phys. Rev. C **63**, 014604 (2000).
 - [25] E. Becheva *et al.*, Phys. Rev. Lett. **96**, 012501 (2006).
 - [26] C. M. Campbell *et al.*, Phys. Lett. B **652**, 169 (2007).
 - [27] Z. Elekes *et al.*, Phys. Rev. C **79**, 011302(R) (2009).
 - [28] N. Aoi *et al.*, Phys. Lett. B **692**, 302 (2010).

- [29] S. Michimasa *et al.*, Phys. Rev. C **89**, 054307 (2014).
- [30] L. A. Riley *et al.*, Phys. Rev. C **90**, 011305(R) (2014).
- [31] A. Corsi *et al.*, Phys. Lett. B **743**, 451 (2015).
- [32] M. L. Cortes *et al.*, Phys. Rev. C **97**, no. 4, 044315 (2018).
- [33] K. Amos, P. J. Dortmans, H. V. von Geramb, S. Karataglidis, and J. Raynal, Adv. Nucl. Phys. **25**, 275 (2000).
- [34] S. Karataglidis, Y. J. Kim and K. Amos, light mass exotic nuclei,” Nucl. Phys. A **793**, 40 (2007) doi:10.1016/j.nuclphysa.2007.06.006
- [35] K. Minomo, K. Ogata, M. Kohno, Y. R. Shimizu and M. Yahiro, J. Phys. G **37**, 085011 (2010).
- [36] M. Toyokawa, K. Minomo, and M. Yahiro, Phys. Rev. C **88**, 054602 (2013).
- [37] M. Toyokawa, M. Yahiro, T. Matsumoto, K. Minomo, K. Ogata and M. Kohno, Phys. Rev. C **92**, no. 2, 024618 (2015) Erratum: [Phys. Rev. C **96**, 059905(E) (2017)].
- [38] K. Minomo, K. Washiyama and K. Ogata, arXiv:1712.10121 [nucl-th].
- [39] K. Egashira, K. Minomo, M. Toyokawa, T. Matsumoto and M. Yahiro, Phys. Rev. C **89**, 064611 (2014).
- [40] K. Minomo and K. Ogata, Phys. Rev. C **93**, 051601(R) (2016).
- [41] Y. Kanada-En’yo and K. Ogata, Phys. Rev. C **99**, no. 6, 064601 (2019).
- [42] Y. Kanada-En’yo and K. Ogata, Phys. Rev. C **99**, no. 6, 064608 (2019).
- [43] Y. Kanada-En’yo, H. Horiuchi and A. Ono, Phys. Rev. C **52**, 628 (1995).
- [44] Y. Kanada-En’yo and H. Horiuchi, Phys. Rev. C **52**, 647 (1995).
- [45] Y. Kanada-En’yo, M. Kimura and A. Ono, PTEP **2012** 01A202 (2012).
- [46] Y. Kanada-En’yo, H. Horiuchi and A. Dote, Phys. Rev. C **60**, 064304 (1999).
- [47] Y. Kanada-En’yo and H. Horiuchi, Phys. Rev. C **68**, 014319 (2003). [nucl-th/0301059].
- [48] Y. Kanada-En’yo and Y. Shikata, Phys. Rev. C **100**, 014301 (2019).
- [49] R. Machleidt, K. Holinde, and Ch. Elster, Phys. Reports **149**, 1 (1987).
- [50] F. A. Brieva and J. R. Rook, Nucl. Phys. A **291**, 299 (1977).
- [51] F. A. Brieva and J. R. Rook, Nucl. Phys. A **291**, 317 (1977).
- [52] F. A. Brieva and J. R. Rook, Nucl. Phys. A **297**, 206 (1978).
- [53] W. Haider, Syed Rafi, J. R. Rook, and Y. K. Gambhir, Phys. Rev. C **93**, 054615 (2016).
- [54] K. Hagino, T. Takehi, and N. Takigawa, Phys. Rev. C **74**, 037601 (2006).
- [55] M. Kamimura, Nucl. Phys. A **351**, 456 (1981).
- [56] J. P. Jeukenne, A. Lejeune and C. Mahaux, Phys. Rev. C **16**, 80 (1977).
- [57] T. Matsumoto, D. Ichinkhorloo, Y. Hirabayashi, K. Katō, and S. Chiba, Phys. Rev. C **83**, 064611 (2011).
- [58] D. Ichinkhorloo, Y. Hirabayashi, K. Katō, M. Aikawa, T. Matsumoto, and S. Chiba, Phys. Rev. C **86**, 064604 (2012).
- [59] H. Guo, Y. Watanabe, T. Matsumoto, K. Nagaoka, K. Ogata, and M. Yahiro, Phys. Rev. C **99**, 034602 (2019).
- [60] T. Matsumoto, J. Tanaka, and K. Ogata, arXiv:1711.07209 (2017).
- [61] Y. Kanada-En’yo, Phys. Rev. Lett. **81**, 5291 (1998).
- [62] Y. Kanada-En’yo, Prog. Theor. Phys. **117**, 655 (2007) Erratum: [Prog. Theor. Phys. **121**, 895 (2009)].
- [63] Y. Kanada-En’yo, Phys. Rev. C **93**, 054307 (2016).
- [64] Y. Kanada-En’yo, Phys. Rev. C **96**, no. 3, 034306 (2017).
- [65] E. Fabrici, S. Micheletti, M. Pignanelli, F. G. Resmini, R. De Leo, G. D’Erasmo and A. Pantaleo, Phys. Rev. C **21**, 844 (1980).
- [66] M. Pignanelli, S. Micheletti, R. De Leo, S. Brandenburg and M. N. Harakeh, Phys. Rev. C **33**, 40 (1986).
- [67] W. Bauhoff *et al.*, Nucl. Phys. A **410**, 180 (1983).
- [68] S. Kato *et al.*, Phys. Rev. C **31**, 1616 (1985).
- [69] S. Kato *et al.*, Nuclear Instruments and Methods **169**, 589 (1980).
- [70] J. Kelly *et al.*, Phys. Rev. Lett. **45**, 2012 (1980).
- [71] H. Ohnuma *et al.*, Nucl. Phys. A **514**, 273 (1990).
- [72] D. R. Tilley, H. R. Weller and C. M. Cheves, Nucl. Phys. A **564**, 1 (1993).
- [73] D. R. Tilley, H. R. Weller, C. M. Cheves and R. M. Chasteler, Nucl. Phys. A **595**, 1 (1995).
- [74] D. R. Tilley, J. H. Kelley, J. L. Godwin, D. J. Millener, J. E. Purcell, C. G. Sheu and H. R. Weller, Nucl. Phys. A **745**, 155 (2004).
- [75] J. H. Kelley, J. E. Purcell and C. G. Sheu, Nucl. Phys. A **968**, 71 (2017).
- [76] H. J. Ong *et al.*, Phys. Rev. C **78**, 014308 (2008).
- [77] B. E. Norum *et al.*, Phys. Rev. C **25**, 1778 (1982).
- [78] J. L. Escudie, R. Lombard, M. Pignanelli, F. Resmini and A. Tarrats, Phys. Rev. C **10**, 1645 (1974) Erratum: [Phys. Rev. C **11**, 639 (1975)].
- [79] M. D. Cortina-Gil *et al.*, Phys. Lett. B **401**, 9 (1997).
- [80] A. A. Korshennikov *et al.*, Phys. Lett. B **343**, 53 (1995).
- [81] L. Grassi *et al.*, J. Phys. Conf. Ser. **381**, 012088 (2012).
- [82] T. Suzuki and T. Otsuka, Phys. Rev. C **56**, 847 (1997).
- [83] A. Navin *et al.*, Phys. Rev. Lett. **85**, 266 (2000).
- [84] S. D. Pain *et al.*, Phys. Rev. Lett. **96**, 032502 (2006).
- [85] N. Imai *et al.*, Phys. Lett. B **673**, 179 (2009).
- [86] R. Meharchand *et al.*, Phys. Rev. Lett. **108**, 122501 (2012).
- [87] A. K. Kerman, H. McManus, and R. M. Thaler, Ann. Phys. **8**, 551 (1959).

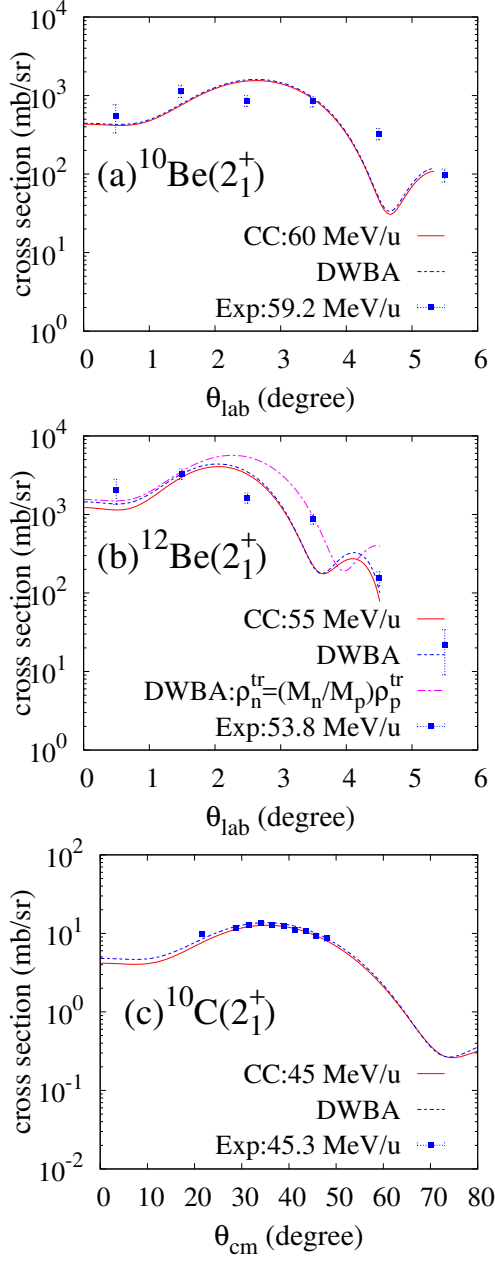


FIG. 11: Cross sections of the inelastic proton scattering to the 2_1^+ state of (a) ^{10}Be at $E = 60$ MeV/u, (b) ^{12}Be at $E = 55$ MeV/u, and (c) ^{10}C at $E = 45$ MeV/u calculated by the CC calculation (red solid lines). The one-step cross sections obtained by the DWBA calculation are also shown (blue dotted lines). In the panel (b) for ^{12}Be , the DWBA calculation using the neutron transition density $\rho_n^{\text{tr}}(r) = (M_n/M_p)\rho_p^{\text{tr}}(r)$ is also shown for comparison (a magenta dash-dotted line). The calculations are compared with the experimental data measured in inverse kinematics of ^{10}Be at 59.2 MeV/u[3], ^{12}Be at 53.8 MeV/u[3], and ^{10}C at 45.3 MeV/u[7]. For the inelastic scattering of ^{10}Be (^{12}Be), θ_{lab} is kinematically limited within 5.6 (4.7) degrees, but the data contain effects of finite size and angular spread of the incident beam, multiple scattering in the target, and detector geometry.

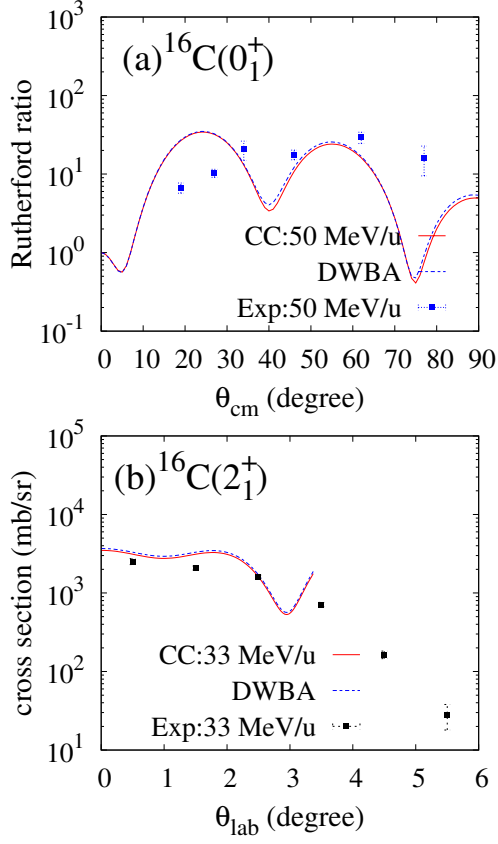


FIG. 12: (a) Cross sections of the elastic proton scattering off ^{16}C at $E = 50$ MeV/u and (b) those of the inelastic scattering at $E = 33$ MeV/u calculated by the CC calculation with the AMD densities (red solid lines). The one-step cross sections obtained by the DWBA calculation are also shown (blue dotted lines). The calculations are compared with the experimental data [9, 81] measured in inverse kinematics. For the inelastic scattering, θ_{lab} is kinematically limited within 3.6 degrees but the data contain effects of finite size and angular spread of the incident beam, multiple scattering in the target, and detector geometry.

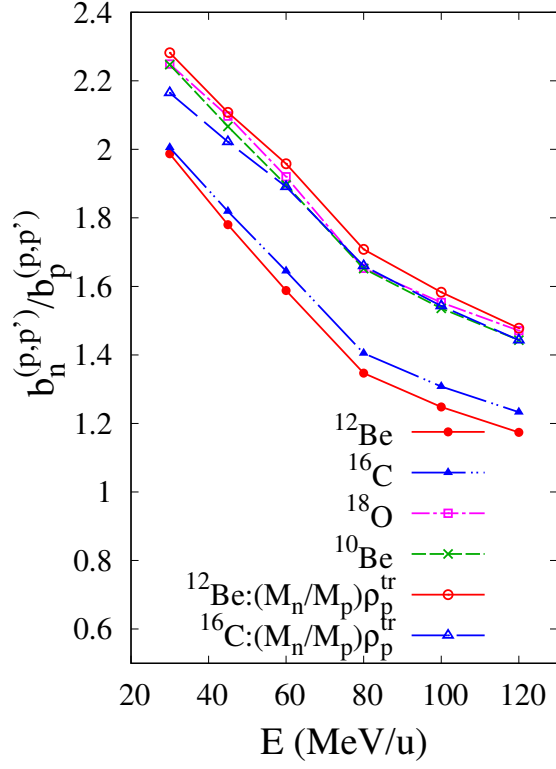


FIG. 13: $b_n^{(p,p')}/b_p^{(p,p')}$ ratio of the proton scattering at $E = 30$ MeV/u, 45 MeV/u, 60 MeV/u, 80 MeV/u, 100 MeV/u, and 120 MeV/u. The values for ^{18}O (magenta open squares), ^{10}Be (green crosses), ^{12}Be (red filled circles), and ^{16}C (blue filled triangles) calculated with the default densities, and those for ^{12}Be (red open circles), and ^{16}C (blue open triangles) of the $\rho_n^{\text{tr}}(r) = (M_n/M_p)\rho_p^{\text{tr}}(r)$ case are shown.